JOURNAL OF SOLID STATE CHEMISTRY 53, 360–368 (1984)

# Idle Spin Behavior of the Shifted Hexagonal Tungsten Bronze Type Compounds $Fe^{II}Fe_2^{III}F_8(H_2O)_2$ and $MnFe_2F_8(H_2O)_2$

M. LEBLANC, G. FEREY, Y. CALAGE,* AND R. DE PAPE

*Laboratoire des Fluorures et Oxyfluorures Ioniques, ERA 609, and *Laboratoire de Spectrométrie Mössbauer, ERA 682, Faculté des Sciences, Route de Laval 72017 Le Mans Cédex, France*

Received July 18, 1983; in revised form November 29, 1983

$Fe^{II}Fe_2^{III}F_8(H_2O)_2$ and $MnFe_2F_8(H_2O)_2$, grown by hydrothermal synthesis ($P \simeq 200$ MPa, $T = 450$ or 380°C), crystallize in the monoclinic system with cell dimensions (Å): $a = 7.609(5)$, $b = 7.514(6)$, $c = 7.453(4)$, $\beta = 118.21(3)°$; and $a = 7.589(6)$, $b = 7.503(8)$, $c = 7.449(5)$, $\beta = 118.06(3)°$, and space group $C2/m$, $Z = 2$. The structure is related to that of $WO_3 \cdot \frac{1}{3} H_2O$. It is described in terms of perovskite type layers of $Fe^{3+}$ octahedra separated by $Fe^{2+}$ or $Mn^{2+}$ octahedra, or in terms of shifted hexagonal bronze type layers. Both compounds present a weak ferromagnetism below $T_N$ (157 and 156 K, respectively). Mössbauer spectroscopy points to an "idle spin" behavior for $Fe^{II}Fe_2^{III}F_8(H_2O)_2$: only $Fe^{3+}$ spins order at $T_N$, while the $Fe^{2+}$ spins remain paramagnetic between 157 and 35 K. Below 35 K, the hyperfine magnetic field at the $Fe^{2+}$ nuclei is very weak: $H_{hf} = 47$ kOe at $T = 4.2$ K. For $MnFe_2F_8(H_2O)_2$, $Mn^{2+}$ spin disorder is expected at 4.2 K. This "idle spin" behavior is due to magnetic frustration.

## Introduction

Hydrothermal synthesis has proved to be very successful for growth of transition metal fluorides (*1*). Low-temperature phases, ammonium compounds, or hydrates are readily obtained by this technique. The hexagonal tungsten bronze type $FeF_3(H_2O)_{0.33}$ (*2*), the modified pyrochlore $NH_4Fe^{II}Fe^{III}F_6$ (*3*), a new form of $NH_4MnFeF_6$ (*4*), recently described, all illustrate the versatility of the method.

Above 400°C, reducing conditions often dominate during hydrothermal experiments when platinum inserts are used. Hydrogen, formed by the reaction of parasitic water with the steel wall of the autoclave, slowly diffuses through the platinum tube. Mixed valence compounds then appear: $Fe^{II}Fe_2^{III}F_8(H_2O)_2$ is thus obtained from $FeF_3$. The corresponding $Mn^{II}$ phase is also synthesized at lower temperature, starting from $MnF_2$ and $FeF_3$.

During editing of this paper, we learned that the structure of $Fe^{II}Fe_2^{III}F_8(H_2O)_2$ was being published by Herdtweck (*5*). Hence, we only briefly present our structural results, which are close to Herdtweck's data. We shall outline the different descriptions of the structure which explain the "idle spin" behavior of these phases; this peculiarity, due to magnetic frustration effects, is deduced from susceptibility, magnetization, and Mössbauer data.

## Experimental

The growth conditions of the compounds of interest in 49% HF are presented in Table I. Good quality single crystals of

0022-4596/84 $3.00

TABLE I

EXPERIMENTAL GROWTH CONDITIONS

| | | $T$ (Å) | $P$ (MPa) | $t$ (hr) |
|---|---|---|---|---|
| $Fe^{II}Fe_2^{III}F_8(H_2O)_2$ | $[FeF_2] = 4\ M$, $[FeF_3] = 4\ M$ | 400 | 205 | 50 |
| | $[FeF_3] = 6\ M$ | 450 | 233 | 120 |
| $MnFe_2F_8(H_2O)_2$ | $[MnF_2] = 5\ M$, $[FeF_3] = 5\ M$ | 380 | 202 | 80 |

$Fe^{II}Fe_2^{III}F_8(H_2O)_2$ were prepared in a platinum tube from $FeF_3$. Crystals as large as 1.5 × 0.7 × 0.5 $mm^3$ were available for single crystal neutron diffraction experiments (accepted at the ILL Institute in Grenoble). When gold tubes are used, $FeF_2$ must be added; under these conditions the crystals are small and poorly crystallized. Isotypic $MnFe_2F_8(H_2O)_2$ crystals are grown with $MnF_2$ replacing $FeF_2$ in the solution.

The stoichiometry of these materials was established by classical chemical analysis of $Fe^{II}$, $Fe^{III}$, Mn, and F (Table II).

Laue and precession photographs show that $Fe^{II}Fe_2^{III}F_8(H_2O)_2$ and $MnFe_2F_8(H_2O)_2$ are monoclinic, with space group $C2/m$ (Table III) and $Z = 2$. Lattice parameters were refined from X-ray patterns obtained from a powder diffractometer (Cu$K\alpha$, internal standard W) (Table III); calculated and observed X-ray spacings of $MnFe_2F_8(H_2O)_2$ are presented in Table IV.

Intensity data were collected on a CAD4 Nonius diffractometer[1] from a single crystal of $Fe^{II}Fe_2^{III}F_8(H_2O)_2$ (reflections measured: total = 1730, $2/m$ symmetry independent and $|F| > 6\sigma(|F|) = 321$). Operating features were as follows: Mo$K\alpha$ radiation; graphite monochromator; scan mode $\omega$, sweep $s = (0.80 + 0.35 \tan\theta)°$; scintillation counter aperture: $D = (1.50 + 1.00 \tan\theta)$ mm; scanning speed $v = (20.1166/NV)°\ min^{-1}$ with

TABLE II

CHEMICAL ANALYSIS (wt%) AND SPECIFIC GRAVITY ($g/cm^3$)

| | $Fe_3F_8(H_2O)_2$ | | $MnFe_2F_8(H_2O)_2$ | |
|---|---|---|---|---|
| | Exp | Calc | Exp | Calc |
| $M^{II}$ | 0.148(12) | 0.157 | 0.172(20) | 0.155 |
| $Fe^{III}$ | 0.318(20) | 0.314 | 0.331(25) | 0.315 |
| F | 0.433(22) | 0.427 | 0.447(25) | 0.429 |
| $\rho$ | 3.19(9) | 3.15 | 3.13(9) | 3.15 |

TABLE III

EXPERIMENTAL DATA FOR $Fe^{II}Fe_2^{III}F_8(H_2O)_2$ AND $MnFe_2F_8(H_2O)_2$

| | | $Fe^{II}Fe_2^{III}F_8(H_2O)_2$ | $MnFe_2F_8(H_2O)_2$ |
|---|---|---|---|
| Symmetry: monoclinic | $a$(Å) | 7.609(5) | 7.589(6) |
| Space group: $C2/m$ | $b$(Å) | 7.514(6) | 7.503(8) |
| Conditions of reflection: | $c$(Å) | 7.453(4) | 7.449(5) |
| $hkl\ h + k = 2n$ | $\beta$(°) | 118.21(3) | 118.06(3) |
| $Z = 2$ | $V$(Å$^3$) | 375.5 | 374.3 |

[1] Laboratoire de Chimie des Solides, L.A. No. 279, U.E.R. de Chimie, Université de Nantes, Nantes, France.

TABLE IV

CALCULATED AND OBSERVED X-RAY SPACINGS FOR $MnFe_2F_8(H_2O)_2$

| $hkl$ | $d_{calc}$ | $d_{obs}$ |
|---|---|---|
| 001 | 6.573 | 6.558 |
| 110 | 4.996 | 5.003 |
| 11$\bar{1}$ | 4.889 | 4.890 |
| 20$\bar{1}$ | 3.791 | 3.789 |
| 020 | 3.752 | 3.758 |
| 111 | 3.439 | 3.440 |
| 200 | 3.349 | 3.348 |
| 002 | 3.287 | 3.287 |
| 021 | 3.258 | 3.262 |
| 20$\bar{2}$ | 3.223 | 3.224 |
| 22$\bar{1}$ | 2.667 | 2.669 |
| 201 | 2.540 | 2.541 |
| 220 | 2.498 | 2.500 |
| 022 | 2.472 | 2.474 |
| 20$\bar{3}$ | 2.431 | 2.433 |
| 112 | 2.388 | 2.390 |
| 31$\bar{1}$ | 2.374 | 2.377 |
| 130 | 2.343 | 2.340 |
| 13$\bar{1}$ | 2.332 | 2.335 |

TABLE V

POSITIONAL AND ISOTROPIC THERMAL PARAMETERS OF $Fe^{II}Fe_2^{III}F_8(H_2O)_2$

| | $x/a^a$ | $x/a^b$ | $y/b^a$ | $y/b^b$ | $z/c^a$ | $z/c^b$ | $B_{eq}{}^a$ (Å$^2$) |
|---|---|---|---|---|---|---|---|
| $Fe^{2+}$ | 0 | | $\frac{1}{2}$ | | 0 | | 0.95(8) |
| $Fe^{3+}$ | $\frac{1}{4}$ | | $\frac{1}{4}$ | | $\frac{1}{2}$ | | 0.73(4) |
| O | 0.2423(9) | 0.2437(4) | 0 | | 0.0435(10) | 0.0412(4) | 3.69(40) |
| F1 | 0 | | 0.2925(7) | 0.2954(2) | $\frac{1}{2}$ | | 1.91(25) |
| F2 | 0.1845(6) | 0.1804(2) | 0 | | 0.4411(7) | 0.4383(2) | 1.42(22) |
| F3 | 0.1277(6) | 0.1292(2) | 0.2952(4) | 0.2979(2) | 0.2138(5) | 0.2142(2) | 1.53(16) |

*Note.* Origin in Herdtweck's work was shifted from $b/2$.

[a] This work.

[b] Herdtwerk's work.

NV integer; range measured: $\theta < 35°$, $0 < h < 10$, $-11 < k < +11$, $-11 < l < +11$ with $C$ restrictions. Corrections for Lorentz and polarization effects and for absorption ($0.712 < A < 0.839$) were applied.

The structure determination was carried out with SHELX program (*6*) using a classical procedure: direct methods, Fourier synthesis, refinement of positional and thermal atomic parameters. It leads to final $R$-factors including the isotropic motion of all non-hydrogen atoms: $R = 0.034$ ($R_W = 0.036$), anisotropic: $R = 0.025$ ($R_W = 0.026$). The results, very close to Herdtweck's work, are specified in Table V, with only the equivalent thermal motion factor. The corresponding interatomic distances are compared in Table VI.

Mössbauer samples contained 5–6 mg/cm$^3$ of natural iron. The spectra given by a triangular wave-form spectrometer were fitted using a least-square method (*7*).

Between 4.2 and 300 K, the susceptibility was measured by the Faraday method; a vibrating sample magnetometer was used to obtain the magnetization data.

TABLE VI

CHARACTERISTIC INTERATOMIC DISTANCES (Å) IN $Fe^{II}Fe_2^{III}F_8(H_2O)_2$

| | This work | Herdtweck's work |
|---|---|---|
| 4x $Fe^{2+}$–F3 | 2.095(3) | 2.081(1) |
| 2x $Fe^{2+}$–O | 2.134(2) | 2.115(3) |
| 2x $Fe^{3+}$–F1 | 1.929(1) | 1.933(1) |
| 2x $Fe^{3+}$–F2 | 1.940(1) | 1.943(1) |
| 2x $Fe^{3+}$–F3 | 1.912(3) | 1.914(1) |

## Discussion of the Structure

Examination of the interatomic distances within the coordination polyhedra clearly points to the fact that:

—cationic order is established between $Fe^{2+}$ and $Fe^{3+}$ (*8*),

—$H_2O$ molecules are placed at the non-bridging vertices of $Fe^{II}$ octahedra (hydrogen atoms are approximately located in Herdtweck's work (*5*)).

The infrared study of $Fe^{II}Fe_2^{III}F_8(H_2O)_2$ provides further support for the presence of these water molecules. The spectrum exhibits an intense and narrow peak at 1650 cm$^{-1}$, and a broad and intense maximum near 3450 cm$^{-1}$. The corresponding absorption may be assigned, respectively, to the bending $\delta_{H_2O}$ and the stretching $\nu_{OH}$ vibrations. The first peak proves that bonded structural water molecules are present. If structural water were coordinated to iron atoms as hydroxyl groups, only the $\nu_{OH}$ peak would be present.

Projections of the structure on the (010) and ($\bar{2}01$) planes are exhibited, respectively, in Figs. 1 and 2. The cationic order

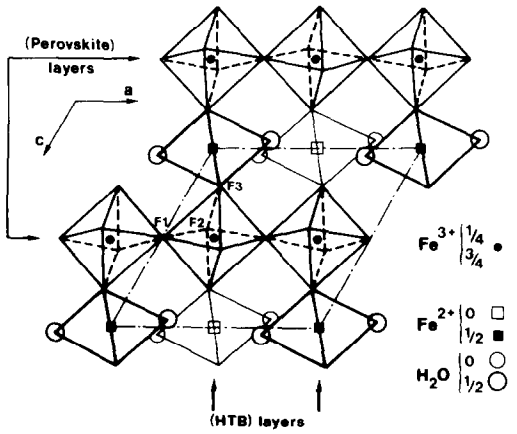


FIG. 1. Projection of $Fe^{II}Fe_2^{III}F_8(H_2O)_2$ along [010]; $Fe^{III}$ octahedra a $y = \frac{1}{4}$ and $y = \frac{3}{4}$ project in identical fashion, but only the chain at $y = \frac{1}{4}$ is drawn.

between $Fe^{2+}$ and $Fe^{3+}$ is shown in Fig. 1. The formation of hexagonal tungsten bronze (HTB) type layers is evidenced by $Fe^{II}Fe_2^{III}F_8(H_2O)_2$ (Fig. 2), similar to the case of $Fe_2F_5$, $2H_2O$, weberite, or of pyrochlore structures. These (HTB) layers are stacked along the [100] direction, with a shift of **b**/2 from one to the next; their connection is ensured by the axial fluorine atoms F1 of the $Fe^{III}F_6$ octahedra. The $H_2O$ molecules occupy the axial positions of $Fe^{II}F_4(H_2O)_2$ octahedra at an equal distance from $Fe^{2+}$ ($d$ = 2.134 Å); they point toward the center of hexagonal cavities of adjacent layers.

This type of structure was first displayed by Gerand *et al.* (*9*) using powder X-ray diffraction data on $WO_3 \cdot \frac{1}{3}H_2O$. In this compound, however, the $WO_4O(H_2O)$ octahedron, just as the $Fe^{II}F_4(H_2O)_2$ octahedron in $Fe^{II}Fe_2^{III}F_8(H_2O)_2$, is in an assymetric environment, with only one long $(H_2O)$–W distance.

Another description of this structure, related to the magnetic behavior, can be provided: the $Fe^{III}F_6$ octahedra buildup, at $z$ = 0.5, infinite perovskite-type layers connected by $Fe^{II}$ octahedra (Fig. 3). The formula may be written as $[Fe^{II}(H_2O)_2]^{2+}[Fe_2^{III}F_8]^{2-}$, and the structure is comparable to that of $AMF_4$ ($A$ = alkaline, $NH_4^+$, $Tl^+$) compounds derived from the $TlAlF_4$ structural type (*10, 11*): namely,

—the water molecules occupy the alkaline ions positions;

—the tilting mode of the $Fe^{III}F_6$ octahedra is $a^-b_p^+c^-$, according to the notation of Glazer (*12*), as modified by Hidaka *et al.* (*13*) for layer compounds;

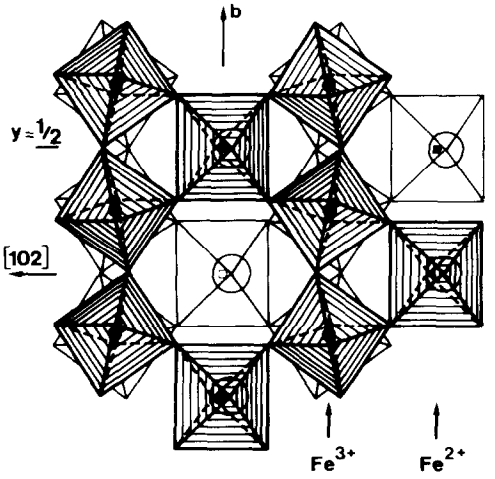


FIG. 2. Projection of $Fe^{II}Fe_2^{III}F_8(H_2O)_2$ along [100] on the $(\bar{2}01)$ plane.

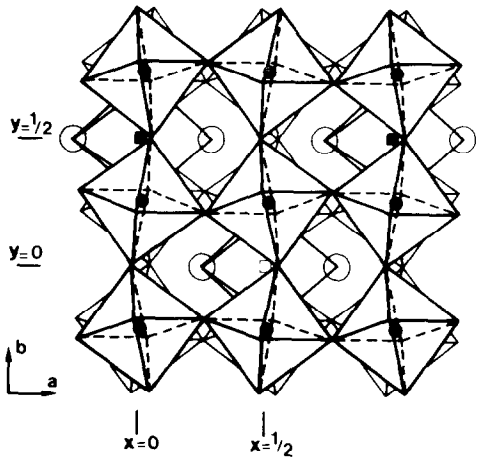


FIG. 3. Projection of $Fe^{II}Fe_2^{III}F_8(H_2O)_2$ along [102] on the (001) plane.

—the equatorial $Fe^{3+}$–$F^-$ distances (1.929 and 1.940 Å) in the perovskite layer plane are slightly longer than axial bonds ($Fe^{III}$–$F_3$ = 1.912 Å); a similar discrepancy is observed in $AMF_4$ compounds.

## Magnetic and Mössbauer Results

$Fe^{II}Fe_2^{III}F_8(H_2O)_2$

Above the magnetic ordering temperature $T_N \simeq 160$ K, the inverse susceptibility (Fig. 4a) obeys a Curie–Weiss law, which leads to $\theta_p = -240 \pm 10$ K and a molar Curie constant of 11.1 ± 0.9 (as compared to the theoretical value $C_m = 11.75$). The relatively high value of $|\theta_p|$ indicates that antiferromagnetic interactions dominate.

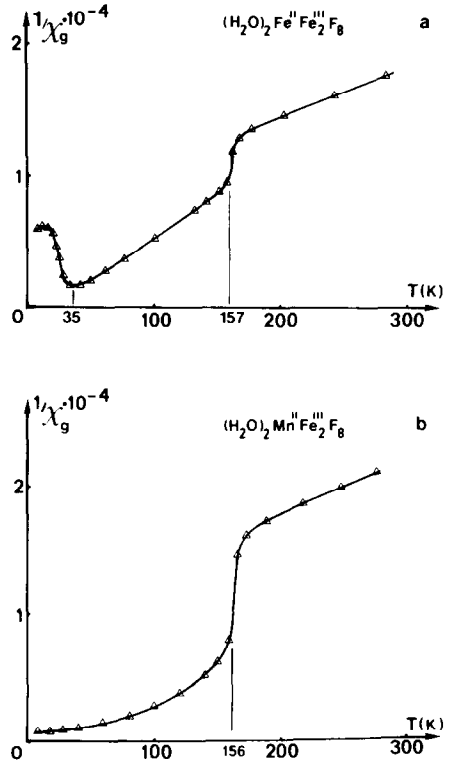


FIG. 4. Thermal variation of the magnetic inverse susceptibility (1/emu $g^{-1}$) of $Fe^{II}Fe_2^{III}F_8(H_2O)_2$ (a) and $MnFe_2F_8(H_2O)_2$ (b).

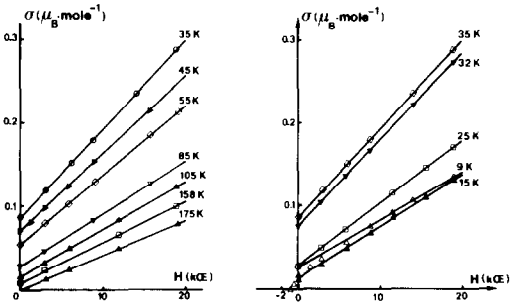


FIG. 5. Magnetization versus the applied field for $Fe^{II}Fe_2^{III}F_8(H_2O)_2$; measurement were performed from 18 to 0 kOe.

Below $T_N$, the variation of the magnetization versus the applied field (Figs. 5 and 6) is consistent with the presence of a weak superimposed ferromagnetism. The coercive field $H_c$ is at a maximum at 35 K ($H_c$ = 1.3 kOe); this low value allows $Fe^{II}Fe_2^{III}F_8(H_2O)_2$ to be considered as a soft magnetic material.

However, a sharp slope inversion of the remanent magnetization $\sigma_r$ (Fig. 7a) and $\chi^{-1}$ curves occurs near 35 K. Only iron Möss-

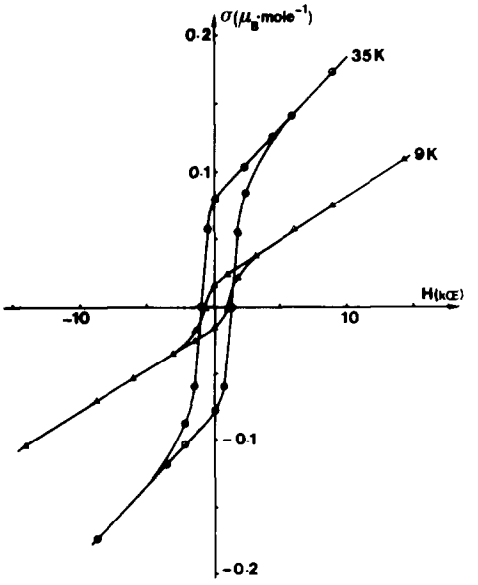


FIG. 6. Hysteresis loop of the ferromagnetic component in $Fe^{II}Fe_2^{III}F_8(H_2O)_2$.

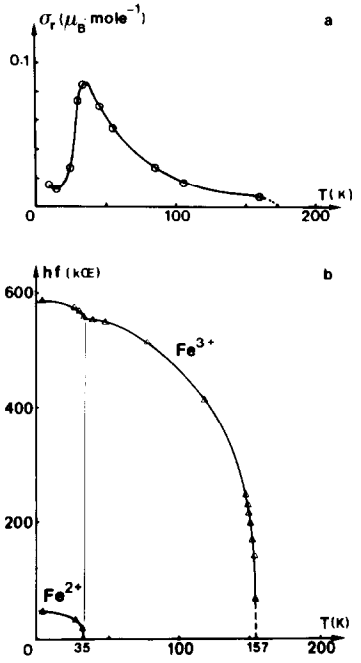


FIG. 7. Thermal variations of the remanent magnetization (a) and the hyperfine fields (b) at $Fe^{2+}$ and $Fe^{3+}$ for $Fe^{II}Fe_2^{III}F_8(H_2O)_2$.

bauer spectrometry provides an explanation of this peculiar feature.

The experimental Mössbauer spectra are presented at Fig. 8 and the corresponding characteristic Mössbauer data are listed in Table VII.

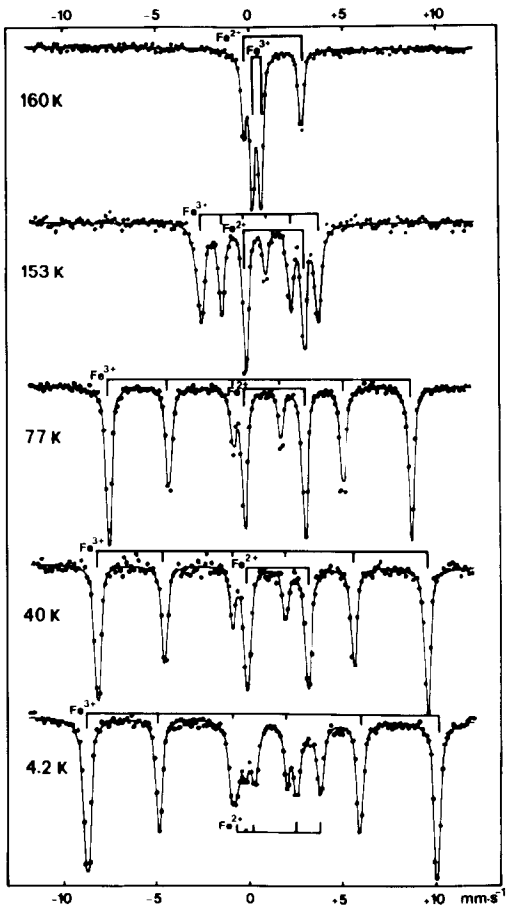


FIG. 8. Mössbauer spectra of $(H_2O)_2Fe^{II}Fe_2^{III}F_8$.

TABLE VII

MÖSSBAUER DATA OF $Fe_3F_8(H_2O)_2$

| | $Fe^{3+}$ | | | | | $Fe^{2+}$ | | | |
|---|---|---|---|---|---|---|---|---|---|
| $T$ (K) | $\delta^a$ (mm · sec$^{-1}$) | $\Delta E_Q$ (mm · sec$^{-1}$) | $4\varepsilon^b$ (mm · sec$^{-1}$) | $H$ (kOe) | $\Gamma$ (mm · sec$^{-1}$) | $\delta^a$ (mm · sec$^{-1}$) | $\Delta E_Q$ (mm · sec$^{-1}$) | $H$ (kOe) | $\Gamma$ (mm · sec$^{-1}$) |
| 295 | 0.467(2) | 0.540(4) | — | — | 0.25(1) | 1.400(2) | 2.216(4) | — | .28(1) |
| 160 | 0.546(2) | 0.431(4) | — | — | 0.31(1) | 1.425(2) | 3.155(4) | — | .28(1) |
| 153 | 0.55(1) | — | 0.38(4) | 199(2) | 0.40(1) | 1.427(2) | 3.175(4) | — | .28(1) |
| 77 | 0.57(1) | — | 0.40(4) | 513(2) | 0.32(1) | 1.472(2) | 3.394(4) | — | .34(1) |
| 40 | 0.57(1) | — | 0.38(4) | 556(2) | 0.32(1) | 1.470(2) | 3.340(4) | — | .40(1) |
| 35 | 0.57(1) | — | 0.39(4) | 560(2) | 0.34(1) | 1.470(2) | 3.336(4) | 0 | .44(1) |
| 33 | 0.58(1) | — | 0.39(4) | 567(2) | 0.32(1) | 1.44(1) | 3.34[c] | 23(3) | .42(1) |
| 4.2 | 0.58(1) | — | 0.33(4) | 586(2) | 0.38(1) | 1.46(1) | 3.34[c] | 47(3) | .42(1) |

[a] Isomer shift relative to Fe metal ($T$ = 300 K).
[b] Quadrupole shift of the outer Zeeman lines.
[c] Fixed values.

Very sharp lines are observed at all temperatures, even close to the magnetic ordering temperature $T_N = 157 \pm 1$ K, established by the thermal scanning method (*14*). The paramagnetic spectrum consists of two well-resolved quadrupole doublets: they are attributed to $Fe^{2+}$ and $Fe^{3+}$ in the molar ratio $Fe^{2+}/Fe^{3+} = 0.53 \pm 0.05$. This value corroborates the stoichiometry.

In the temperature range 157–35 K, the magnetic ordering on the $Fe^{3+}$ site is established by the characteristic Zeeman sextet, while the quadrupole doublet of $Fe^{2+}$ remains unchanged. Below 35 K, this last doublet disappears and the spectra are fitted using two magnetic sextets. The thermal variations of the magnetic hyperfine fields at Fe nuclei (Fig. 7b) quantify these observations: it is clear that the magnetic ordering of $Fe^{2+}$ occurs only for $T < 35$ K. This order influences the magnetic hyperfine field at the $Fe^{3+}$ site and, as already mentioned, the susceptibility and the remanent magnetization decrease strongly.

### $MnFe_2F_8(H_2O)_2$

The paramagnetic portion of the inverse susceptibility curve (Fig. 4b) leads to $\theta_p = -240 \pm 20$ K and $C_{exp} = 11.0 \pm 1.0$ (compared to the theoretical value $C_m = 13.12$). Below $T_N$, the inverse susceptibility decreases in a regular manner; a weak superimposed ferromagnetism appears (Fig. 9). In contrast with $Fe^{II}Fe^{III}_2F_8(H_2O)_2$, the remanent magnetization varies monotonically with temperature (Fig. 10a).

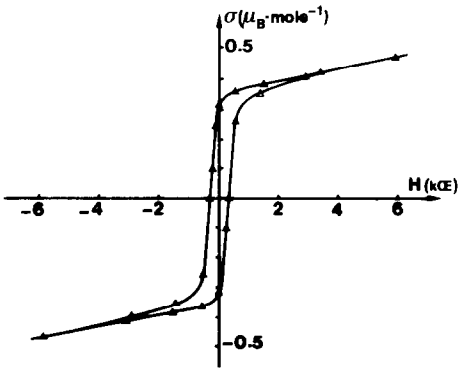


FIG. 9. Hysteresis loop of the ferromagnetic component in $MnFe_2F_8(H_2O)_2$ at $T = 9$ K.

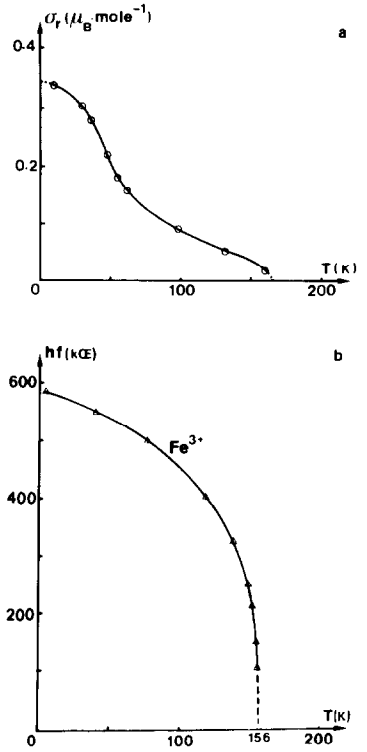


FIG. 10. Thermal variations of the remanent magnetization (a) and the hyperfine field (b) at $Fe^{3+}$ for $MnFe_2F_8(H_2O)_2$.

The iron Mössbauer spectrometry provides an accurate determination of $T_N = 156 \pm 1$ K. The very simple spectra are characteristic of $Fe^{3+}$: a quadrupole doublet and a magnetic sextet, respectively, above and below $T_N$. No sharp variation of the magnetic hyperfine field (Fig. 10b) was observed at low temperature; its value at 4.2 K (585 ± 2 kOe) (Table VIII) is identical to that of $Fe^{II}Fe^{III}_2F_8(H_2O)_2$ (586 ± 2 kOe).

## Discussion

The most important feature of this work is the "idle spin" behavior of the magnetic

TABLE VIII

MÖSSBAUER DATA OF $MnFe_2F_8(H_2O)_2$

| $T$ (K) | $\delta^a$ (mm · sec$^{-1}$) | $\Delta E_Q$ (mm · sec$^{-1}$) | $4\varepsilon^b$ (mm · sec$^{-1}$) | $H$ (kOe) | $\Gamma$ (mm · sec$^{-1}$) |
|---|---|---|---|---|---|
| 295 | 0.473(2) | 0.545(4) | — | — | 0.28(1) |
| 157.5 | 0.548(2) | 0.474(4) | — | — | 0.31(1) |
| 153 | 0.54(1) | — | −0.87(4) | 205(2) | 0.50(1) |
| 77 | 0.57(1) | — | −0.86(4) | 498(2) | 0.36(1) |
| 4.2 | 0.59(1) | — | −0.70(4) | 585(2) | 0.32(1) |

[a,b] Remarks of Table VII.

phase of $Fe^{II}Fe^{III}_2F_8(H_2O)_2$ between 157 and 35 K: the $Fe^{2+}$ magnetic moments remain in the paramagnetic state, whereas the $Fe^{3+}$ sublattice is magnetically ordered. These latter ions lie in the perovskite planes described above (Fig. 3). Thus, $Fe^{II}Fe^{III}_2F_8(H_2O)_2$ may be considered as a 2-D magnetic material in this temperature range. However, the relatively high value of $T_N$, compared to that of the $AMF_4$ compounds, implies that the magnetic layers are strongly coupled by the $Fe^{2+}$ spins.

Preliminary information concerning spin orientation just below $T_N$ is expected from the quadrupole shift values under the assumption of an axial electric field gradient (EFG). On analyzing these values close to $T_N$, the angle $\theta$ between the main EFG axis and the magnetic hyperfine field direction may be derived. In the case of $MnFe_2F_8(H_2O)_2$, the value $\theta \simeq 0°$ is unambiguously calculated and $\Delta E_Q$ is negative. For $Fe^{II}Fe^{III}_2F_8(H_2O)_2$, two possible $\theta$ values occur: $\theta \simeq 90°$ ($\Delta E_Q < 0$) or $\theta \simeq 36°$ ($\Delta E_Q > 0$). Both compounds are isostructural, so it is likely that $\Delta E_Q$ is negative for both cases, and that the main EFG axis is along the same orientation. Then, $\theta$ values are $\theta \simeq 90°$ for $Fe^{II}Fe^{III}_2F_8(H_2O)_2$ and $\theta \simeq 0°$ for $MnFe_2F_8(H_2O)_2$. Thus, just below $T_N$ the directions of $Fe^{3+}$ magnetic moments would differ for these compounds. However, the particular $\theta$ values (0° or 90°) are consistent with $Fe^{3+}$ spins that are either parallel or perpendicular to the perovskite-type planes described above; this last case is always encountered in $AFeF_4$ compounds ($A$ = K, Cs) (*15*, *16*).

At $T < 35$ K the Mössbauer spectra of $Fe^{II}Fe^{III}_2F_8(H_2O)_2$ were fitted using a fixed absolute value of the quadrupole shift $\Delta E_Q$ for $Fe^{2+}$. Depending on the sign of $\Delta E_Q$, the fitted $\theta$ parameter is approximately 70° ($\Delta E_Q < 0$) or 35° ($\Delta E_Q > 0$), with the asymmetry parameter $\eta$ assumed to be zero.

The hyperfine field $H_{hf}$ at $Fe^{2+}$ ion is very weak (47 ± 3 kOe at 4.2 K) compared to that encountered in fluorinated bronzes: 240–330 kOe (*17*). However, it should be compared to that found in $Fe_2F_5, 2H_2O$ where $H_{hf} = 41.1$ kOe (*18*).

This similarity is related to the existence in both structures of triangular arrays formed by one $Fe^{2+}$ and two $Fe^{3+}$ octahedra linked by corners. These units are part of hexagonal bronze type layers (presented in Fig. 2 for $Fe^{II}Fe^{III}_2F_8(H_2O)_2$. The antiferromagnetic interactions (*19*) cannot all be satisfied. Strong coupling between $Fe^{3+}$ arise, and the antiferromagnetic exchange between $Fe^{3+}$ and $Fe^{2+}$ is thereby constrained. In $Fe_2F_5, 2H_2O$, Mössbauer spectroscopy shows that $Fe^{2+}$ and $Fe^{3+}$ magnetic sublattices order at the same temperature. $Fe^{II}Fe^{III}_2F_8(H_2O)_2$ behaves differently: the frustration is minimized by maintaining the $Fe^{2+}$ spins in the paramagnetic state (35 K $< T <$ 157 K). In this last struc-

ture, when $Mn^{2+}$ occupy the $Fe^{2+}$ positions, only identical $d^5$–$d^5$ interactions occur; the absence of any strange features of the $\chi^{-1}$, $\sigma_R$, and $H_{hf}$ curves leads to the supposition that $MnFe_2F_8(H_2O)_2$ is also an "idle spin" compound.

A planned determination of the magnetic structures will be necessary to characterize the type of frustration adopted in these three compounds (*20*).

## Acknowledgments

The authors are very indebted to Dr. Chevallier (L.A.279 Nantes) for X-ray data collection.

## References

1. G. Ferey, M. Leblanc, R. De Pape, M. Passaret, and M. P. Bothorel-Razazi, *J. Cryst. Growth* **29,** 209 (1975).
2. M. Leblanc, G. Ferey, P. Chevallier, Y. Calage, and R. De Pape, *J. Solid State Chem.* **47,** 53 (1983).
3. G. Ferey, M. Leblanc, and R. De Pape, *J. Solid State Chem.* **40,** 1 (1981).
4. M. Leblanc, G. Ferey, Y. Calage, and R. De Pape, *J. Solid State Chem.* **47,** 24 (1983).
5. E. Herdtweck, *Z. Anorg. Allg. Chem. 501-6,* 131 (1983).
6. G. M. Sheldrick, "SHELX. A Program for Crystal Structure Determination," Univ. of Cambridge, England (1976).
7. J. Teillet and F. Varret, unpublished computer programs.
8. R. D. Shannon, *Acta Crystallogr. Sect. A* **32,** 751 (1976).
9. B. Gerand, G. Nowogrocki, and M. Figlarz, *J. Solid State Chem.* **38,** 312 (1981).
10. C. Brosset, *Z. Anorg. Allg. Chem.* **239,** 301 (1938).
11. J. L. Fourquet, F. Plet, G. Courbion, A. Bulou, and R. De Pape, *Rev. Chim. Minér.* **16,** 490 (1979).
12. A. M. Glazer, *Acta Crystallogr. Sect. A* **31,** 756 (1975).
13. M. Hidaka, I. G. Wood, B. M. Wanklyn, and B. J. Garrard, *J. Phys. C* **12,** 1799 (1979).
14. G. Ferey, R. De Pape, and F. Varret, *J. Phys. Colloq.* **38** C7, 107 (1977).
15. G. Heger, R. Geller, and D. Babel, *Solid State Commun.* **9,** 335 (1971).
16. D. Babel, F. Wall and G. Heger, *Z. Naturforsch. B* **29,** 131 (1974).
17. N. N. Greenwood, F. Menil, and A. Tressaud, *J. Solid State Chem.* **5,** 402 (1972).
18. P. Imbert, G. Jehanno, Y. Macheteau, and F. Varret, *J. Phys.* **37,** 969 (1976).
19. J. Kanamori, *J. Phys. Chem. Solids* **10,** 87 (1959).
20. G. Toulouse, *Commun. Phys.* **2,** 115 (1977).